Turk J Phys
32 (2008) , 105 – 114.

Photoelectrochemical Investigations on $Hg_xCd_{1-x}Se$ Thin Film Electrode/Electrolyte System

Vithal Bhivaba PUJARI[1] **and Lalasaheb Patangrao DESHMUKH**[2]
[1] *Rayat Shikskan Sanstha's, Karmaveer Bhaurao Patil College, Vashi, Navi-Mumbai 400703, M. S., INDIA*
e-mail: vbpmodphy@yahoo.co.in
[2] *Thin Film and Solar Studies Research Laboratory, Department of Physics (Applied Electronics), Solapur University, Solapur, Solapur - Pune Road, Kegaon, Solapur 413255, M. S., INDIA*

Received 2007

Abstract

Thin film electrodes of $Hg_xCd_{1-x}Se$ ($0 \leq x \leq 0.2$) were prepared in an aqueous alkaline medium (pH $\cong$ 11) on highly conducting stainless steel substrates by chemical bath technique. Use of these films was made as an active photoelectrode in an electrochemical photovoltaic cell, comprising: electrode; sodium polysulphide electrolyte; and impregnated graphite as a counter electrode. The investigations on these cells were made by studying I-V and C-V characteristics in dark, power output, built-in-potential, spectral and photo responses. Cell performance parameters were evaluated: open-circuit photopotential V_{ph}; and short-circuit photocurrent I_{ph}; series and shunt resistances R_s and R_{sh}; quantum conversion efficiency η; fill factor *ff*; junction ideality factor n_d; light quality factor n_L; built-in-potential Φ_B; and the flat-band potential V_{fb} were evaluated. Careful inspection of calculated values of these parameters revealed that the cell performance has been greatly enhanced with increasing electrode composition. Typically, the quantum conversion efficiency and fill factor are found to be enhanced from 0.056% to 0.31% and 31% to 52% respectively, as the photoelectrode composition varied from zero to 0.01. Incremental changes in the performance parameters, and consequently the enhancement in the cell performance are explained on the basis of electrode materials composition.

Key Words: MCS, P-V cells, efficiency and fill factor.

1. Introduction

Pseudobinaries of II-VI and IV-VI semiconductors, especially cadmium chalcogenides, are currently becoming the focus of intensive research as they exhibit potential as efficient absorbers in the visible and near infrared regions of the solar spectrum [1-3]. The action spectra of these materials show a good deal of enhancement over a wide range of photon energies. Cadmium Selenide is such a semiconducting material, which has shown a great promise for photoelectrochemical conversion [3-5]. With this material, a relatively large fraction of the solar spectrum can be utilized and it is, therefore, reasonable to expect a considerable improvement in the quantum conversion efficiency. The conversion efficiencies so far reported are low compared with other materials such as $CuInSe_2$, $CuInS_2$, $CuIn(Se,S)_2$ etc., and one of the prominent reasons pointed out by many researchers is the unmatched electrode resistivity [1-5]. Resistivity of active electrode

materials could be made to match by incorporating trace amount of impurities in the host lattice. Impurities like indium, antimony, arsenic, bismuth, phosphor etc., have shown pronounced effects in a number of host lattices [6-9]. In these investigations, therefore, it is proposed to incorporate mercury in CdSe host-lattice and to study its effects on the electrochemical performance of a cell made from these photoelectrodes.

2. Experimental Details

2.1. Preparation of $Hg_xCd_{1-x}Se$ photoelectrodes

Thin film electrodes of $Hg_xCd_{1-x}Se$ ($0 \leq x \leq 0.2$) were obtained on the well-processed stainless steel and glass substrates using a simple chemical bath technique [9-12]. For the synthesis, A.R. grade solutions of 1 M Cadmium Chloride, 1 M Mercuric Chloride and refluxed sodium selenosulphite were taken together and complexed with a sufficient quantity of triethanolamine. Sodium hydroxide and aqueous ammonia were used to adjust the pH (11±0.2) of the resulting mixture and to ensure better adherence of film samples to the substrates. The cleaned substrates were then positioned on a substrate holder and kept rotating at speed 60 ± 2 rpm in the reaction mixture, which was maintained at 60 ^oC. Deposition was carried out over 90 min; then the samples were taken out of the reaction mixture, washed with double distilled water and preserved in dark.

2.2. Fabrication and characterization of photoelectrochemical cells

The photoelectrochemical (PEC) cell was fabricated in an H-shaped glass cuvette using one of the samples as an active photoelectrode, sodium polysulphide redox electrolyte, and impregnated graphite rod as a counter electrode. The power output characteristics were obtained for all the cell configurations under a constant input light intensity of 20 $mWcm^{-2}$ (supplied by a 250W tungsten filament lamp). A potentiometric arrangement in a two-electrode system was used for this purpose. The generated photo potentials and photocurrents were noted for various illumination intensities (from 5 to 20 $mWcm^{-2}$). The spectral responses of the various detector systems were examined in the range of wavelengths from 400 nm to 1300 nm. The dynamic I-V and C-V characteristics in dark were obtained potentiometrically for all cells. Three-electrode system was used for the capacitance-voltage measurements. A saturated calomel electrode (SCE) was used as reference. The reverse saturation current of the various cells was noted in the 373 to 300 K temperature range to calculate the built-in-potentials of the various cells. The various photocurrents and photovoltages were measured by $6^1/_2$ digit HP and $4^1/_2$ digit HIL 2665 multimeters. Illumination intensities were recorded by a Lutron-101 (Taiwan) luxmeter. A ten-turn 1-kohm helical potentiometer was used to vary the junction potential. A Cameca SU-30 scanning electron microscope (France) was used to observe the surface morphology.

3. Results and Discussion

3.1. Physical observations

The as-grown samples were thin, relatively uniform, pin hole free, mechanically hard, diffusely reflecting and tightly adherent to the substrate support with colour changing from dark orange red to lead gray as Hg-content was increased from 0 to 0.2. The change in colour is indicative of the replacement of Cd^{2+} by Hg^{2+} in the CdSe-lattice. The composition dependent growth mechanism was studied and it has been observed that, the photoelectrode thickness decreased monotonically and nonlinearly with the photoelectrode composition as shown in Figure 1 and explained on the similar lines to those reported earlier [10, 11].

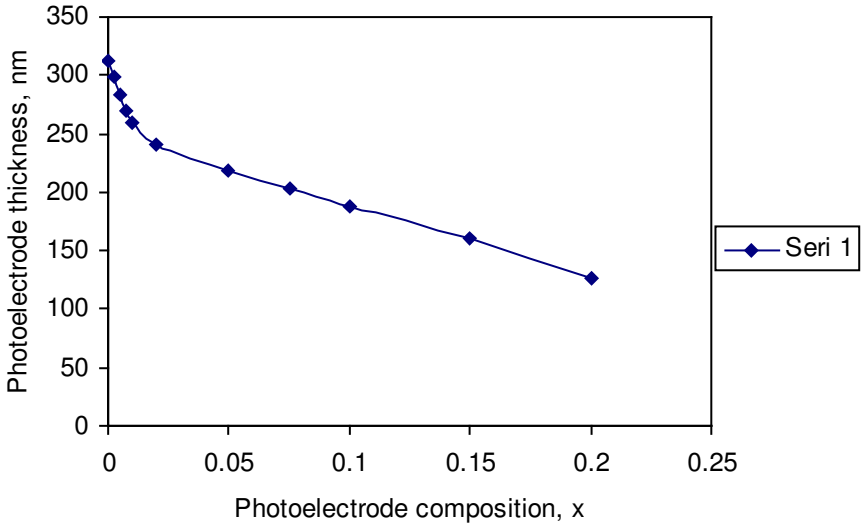

Figure 1. Thin film photoelectrode thickness decreases monotonically with photoelectrode composition x.

3.2. The photoelectrochemical (PEC) cells

The electrochemical cells set in a glass cuvette with $Hg_xCd_{1-x}Se$ ($0 \leq x \leq 0.2$) photoelectrodes and sodium polysulphide as an electrolyte were devised and illuminated by a white light of intensity 20 mW cm^{-2}. The excess charge carriers, which are generated as a result of the photon absorption in the active region of the electrode/electrolyte interface are separated; the electrons move deep into the bulk, while holes arrive at the surface of the semiconductor electrode causing redox reactions to occur. The charge separation process continues until it results in a counter field, which is maximum at the open-circuit condition called open circuit photopotential [12-15].

The photo responsiveness of these cells was therefore studied under a variable input light intensity from 5 to 20 mWcm^{-2}. The photopotentials (V_{ph}) and photocurrents (I_{ph}) were recorded as a function of the input intensity. The open-circuit photopotential is an approximately linear function of the input light intensity as shown in Figure 2 for six typical cell configurations.

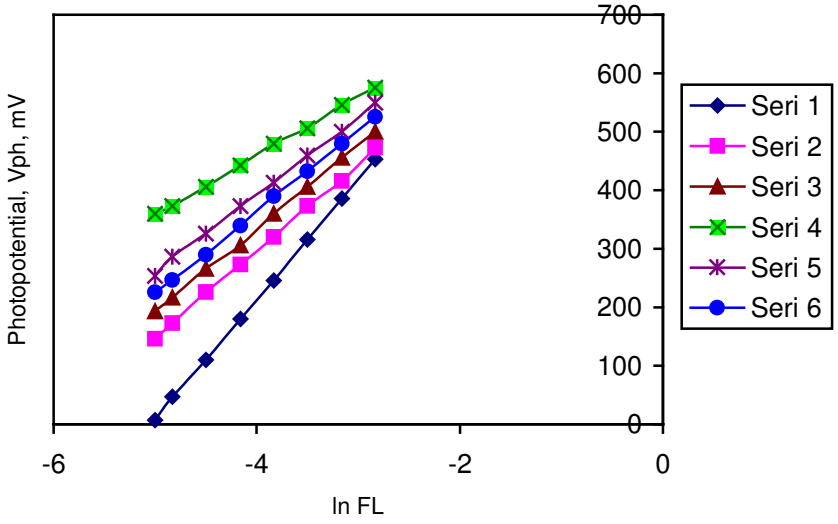

Figure 2. Variation of photopotential V_{ph} with input light intensity for six typical photoelectrode compositions: a) x = 0(♦), b) x = 0.005(■), c) x = 0.0075(▲), d) x = 0.01(×), e) x = 0.02(∗) and f) x = 0.05(●).

The linear dependence of the short-circuit photocurrent demonstrates that the transport of electroactive species to the electrode/electrolyte interface does not limit the rate of the overall charge transfer reaction [13-15]. The open-circuit photopotential initially varies quasi-linearly and then tends to saturate at high levels of illumination intensities.

Under illumination, the I-V characteristic can be represented via the relation

$$I = I_{ph} - I_d = I_{ph} - I_o[\exp(qV/n_d kT) - 1], \tag{1}$$

where symbols have their usual physical significance. For bias voltages exceeding 3kT/q and in the equilibrium open- circuit conditions

$$I_{ph} = I_d, V = V_{ph}, \tag{2}$$

equation (1) can be rearranged as

$$V_{ph} \approx (n_L kT/q) ln(I_{ph}/I_o). \tag{3}$$

Since $I_{ph} >> I_o$,

$$V_{ph} \alpha (n_L kT/q) ln F_L. \tag{4}$$

A plot of V_{ph} versus ln F_L would be a straight line and n_L may be calculated form its slope. The light quality factors n_L of the various junctions was therefore computed from these plots and is listed in Table.

Table. Various PEC cell performance parameters of $Hg_xCd_{1-x}Se$ thin film photoelectrodes.

Photo-electrode composition x	n_d	n_L	I_o μA	Φ_B, eV	V_{ph}, mV	I_{ph}, μA	R_s, Ω	R_{sh}, kΩ	Crystallite size, nm	
									XRD	SEM
0.00	3.06	2.63	5.2	0.37	343	105	1800	4.48	177	463
0.0025	2.75	2.37	6.3	0.39	369	113	1768	4.80	183	474
0.0050	2.52	2.16	8.3	0.45	414	145	1028	7.36	189	496
0.0075	2.43	1.94	16.6	0.53	450	165	720	7.94	196	512
0.01	1.97	1.52	84.9	0.69	546	223	368	9.06	203	532
0.02	2.15	1.89	50.0	0.63	504	203	385	8.12	218	567
0.05	2.38	2.10	31.6	0.58	474	187	400	7.98	258	670
0.075	2.47	2.26	21.9	0.55	465	178	423	7.75	253	664
0.10	2.64	2.30	14.1	0.47	432	152	867	7.42	247	656
0.15	2.68	2.35	11.2	0.44	402	137	1095	7.00	249	661
0.20	2.72	2.39	9.9	0.41	387	122	1270	6.00	248	668

The power output curves (Figure 3) were obtained for the cells with seven typical photoelectrode compositions. The cell parameters, viz. open-circuit photopotential V_{ph}, short-circuit photocurrent I_{ph}, quantum conversion efficiency η, fill factor ff, series and shunt resistances R_s and R_{sh}, were determined. Both the open-circuit photopotential and short-circuit photocurrent have been found to be boosted from 343 mV and 105 μA to 546 mV and 223 μA at x = 0.01. Both the photopotentials and photocurrents have been found to be increased significantly at x = 0.01, but decreased thereafter. We attribute the observed improvements in V_{ph} and I_{ph} mainly to the decreased series resistance, increased photosensitivity, improved grain structure and decreased band gap [14-16].

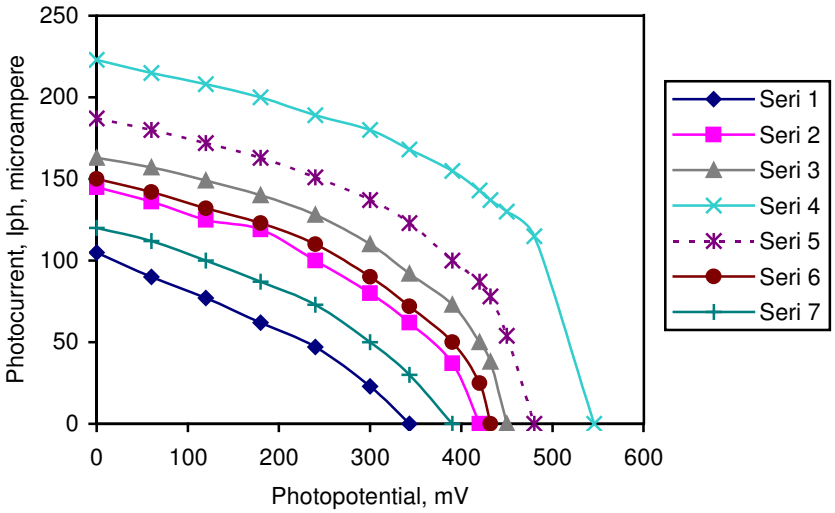

Figure 3. Power output curves for the cells with seven typical photoelectrode compositions: a) x = 0(♦), b) x = 0.005(■), c) x = 0.0075(▲), d) x = 0.01(×), e) x = 0.05(∗), f) x = 0.1(●) and g) x = 0.2(+).

Variations in quantum conversion efficiency η and fill factor ff with Hg content in the host CdSe-lattice are shown in Figures 4(a) and 4(b), respectively. In general, to explain this variation of η and ff, we should consider the materials characteristics such as band gap E_g and the flat-band potential V_{fb}. Efficiency has a direct relation to the flat-band potential, whereas it varies reciprocally with the band gap [15, 16]. In our case, the cell delivered a maximum quantum conversion efficiency of 0.31% at x = 0.01 and could obviously be due to a larger value of the flat-band potential (-945 mV) and the optimum value of the band gap (1.53 eV) at x = 0.01.

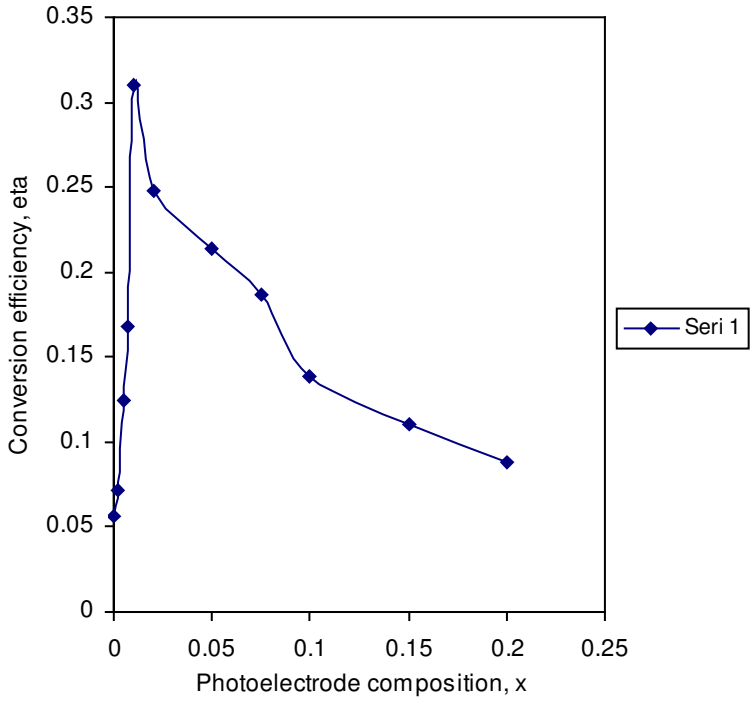

Figure 4a. Variation of quantum conversion efficiency η (%) with photoelectrode composition x.

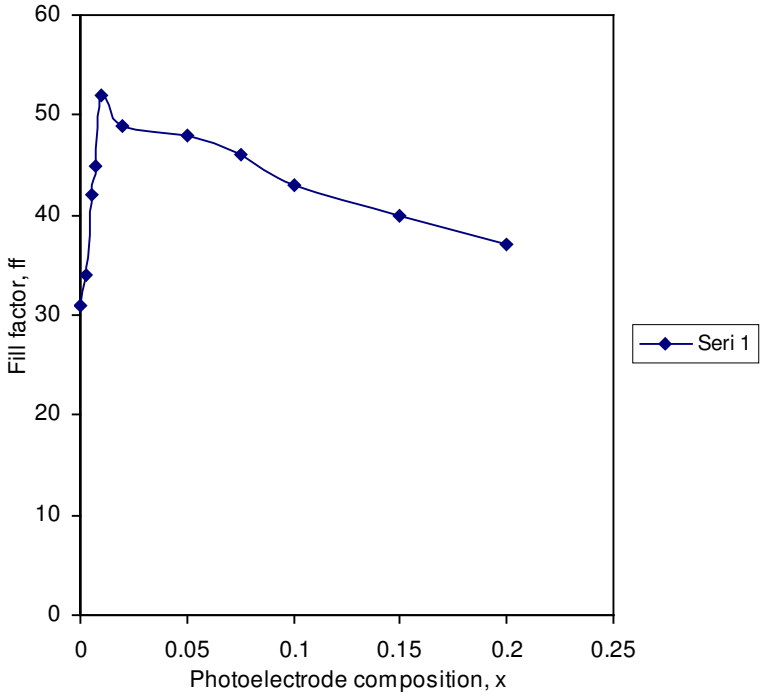

Figure 4b. Variation of fill factor ff (%) with photoelectrode composition x.

The photoaction spectra (spectral responses) were examined for the selected cells out of the series of these cells. It is found that the cell has comparatively broader spectral response, and that response edge of the cell at longer wavelength is not sharp with the clear appearance of response tail. The action spectra for four typical cells are shown in Figure 5. From this, it is clear that the photocurrent increased with incident wavelength and maximized at the cutoff wavelength λc, 720 nm and 810 nm for the PEC cells with compositions, x = 0 (pure CdSe) and x = 0.01 (optimum composition) respectively. Thereafter the photocurrent decreased for higher wavelengths. However, the longer wavelength cutoff is not sharp, which is a common experience with the polycrystalline thin film photoelectrochemical cells and the short-circuit photocurrent for the cell with electrode composition, x = 0.01 is larger indicating a lower trap density at the electrode / electrolyte interface for this cell.

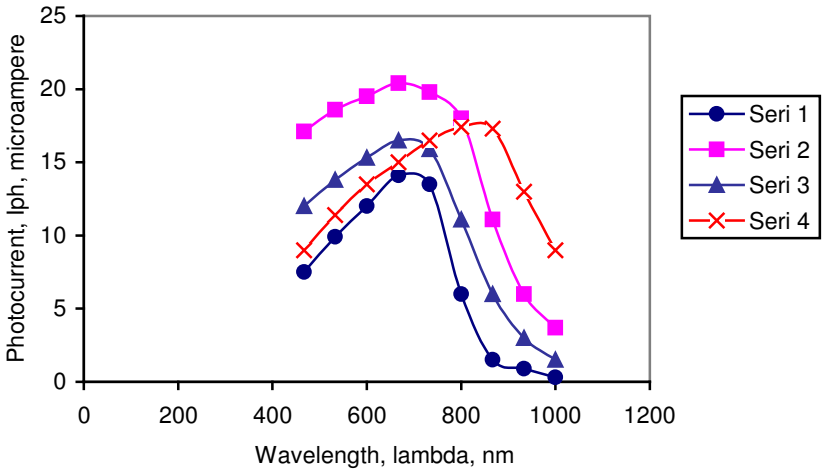

Figure 5. Photo action spectra of four typical cells with the photoelectrode composition: a) x = 0(●), b) x = 0.005(▲), c) x = 0.01(■) and d) x = 0.05 (×)

The overall observed improvement in the PEC performance could also be understood and supported by the following characteristic properties of the various cells and the electrode material. The current-voltage and capacitance-voltage (versus SCE) characteristics in the dark were therefore studied and analyzed for the series of cells. Plots of log I_{ph} versus V_{ph} for six typical cells is shown in Figure 6 and the junction ideality factor n_d for all the cell structures are determined from the high-voltage regions (linear) of these plots. The conventional reverse saturation current I_o was also determined from these plots and listed in Table. It is seen that n_d decreased typically from 3.06 to 1.97 as x varied from 0 to 0.01. For higher values of x, n_d increased. It is presumed that there is a considerable recombination at the interface and is minimum for the cell formed with photoelectrode composition, x = 0.01.

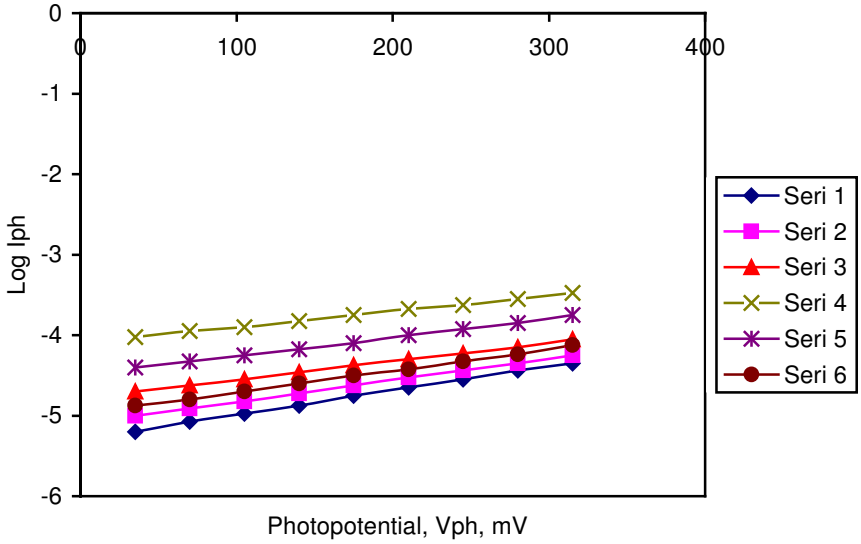

Figure 6. Variation of n_d from log I versus V variations for six typical cells: a) x = 0(♦), b) x = 0.005(■), c) x = 0.0075(▲), d) x = 0.01(×), e) x = 0.05(∗) and f) x = 0.1(●).

A second important characteristic of an electrode/electrolyte interface is the voltage-dependent space-charge layer capacitance. This characteristic gives an important insight about the relative positions of the Fermi levels of a semiconductor and an electrolyte redox couple that determine the amount of band bending at the interface, which is the measure of the flat-band potential or a maximum value of the open-circuit photopotential V_{ph} that can be attainable from a cell. The flat-band potentials (V_{fb}) were therefore determined for all the cells of different photoelectrode compositions by measuring the space-charge layer capacitance under a reverse-bias voltage (versus SCE). The C^{-2} versus V (versus SCE) plots were then constructed for all the cells and extrapolated to the voltage-axis to get the flat-band potentials. The values of V_{fb} are plotted against the photoelectrode composition x and are shown in Figure 7. It is notable that V_{fb} increased considerably with photoelectrode composition, x, attained a maximum value at x = 0.01 and then decreased for higher values of x. The increase in V_{fb} is caused mainly by the additional donor levels, which effectively shift the Fermi level contributing to the increased V_{ph} of a cell whereas the decay of V_{fb} at higher values of x, may be due to pinning of the Fermi level [12, 16]. This is further supported by the built-in-potential (Φ_B) measurement on the various cells. The Φ_B values are listed in Table.

A direct correlation can also be made between the electrochemical performance of the various cells and some of the materials properties of the photoelectrode. The scanning electron micrographs (SEM) (see Figure 8) and X-ray diffractograms (XRD) were used to ascertain the surface features and crystal dimensions. It has been seen that the crystallite size is enhanced up to a value of electrode materials composition x = 0.01 and then decreased for further increase in the x-values. The crystallite sizes calculated from the SEM and XRD observations are listed in the Table. It is observed that there is a lack of good agreement

between crystallite sizes calculated from XRD patterns and SEM observations may be due to agglomeration of the crystallites to form a particle, obviously showing bigger sizes [11]. The improved crystallite structure, decreased band gap, increased photoelectrode absorption and electrical conductivity caused the series resistance R_s of a photoelectrochemical cell to decrease resulting in the increased photocurrent and hence the quantum conversion efficiency.

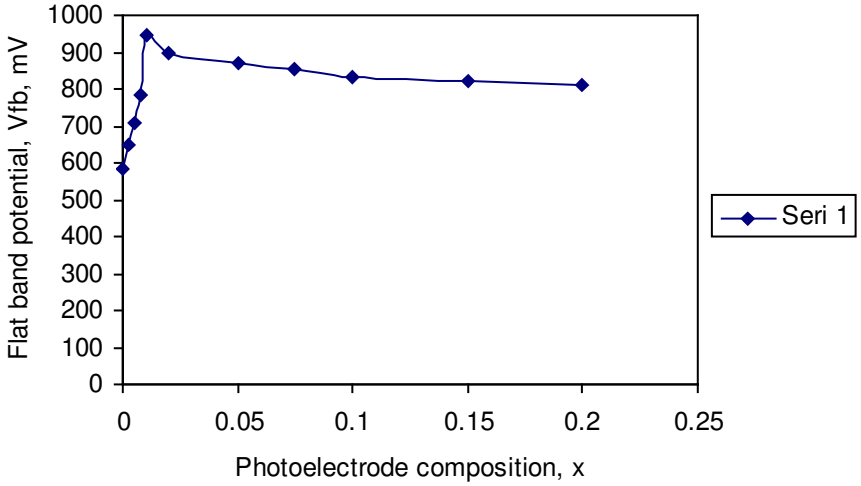

Figure 7. Variation of flat-band potential V_{fb} with photoelectrode composition, x.

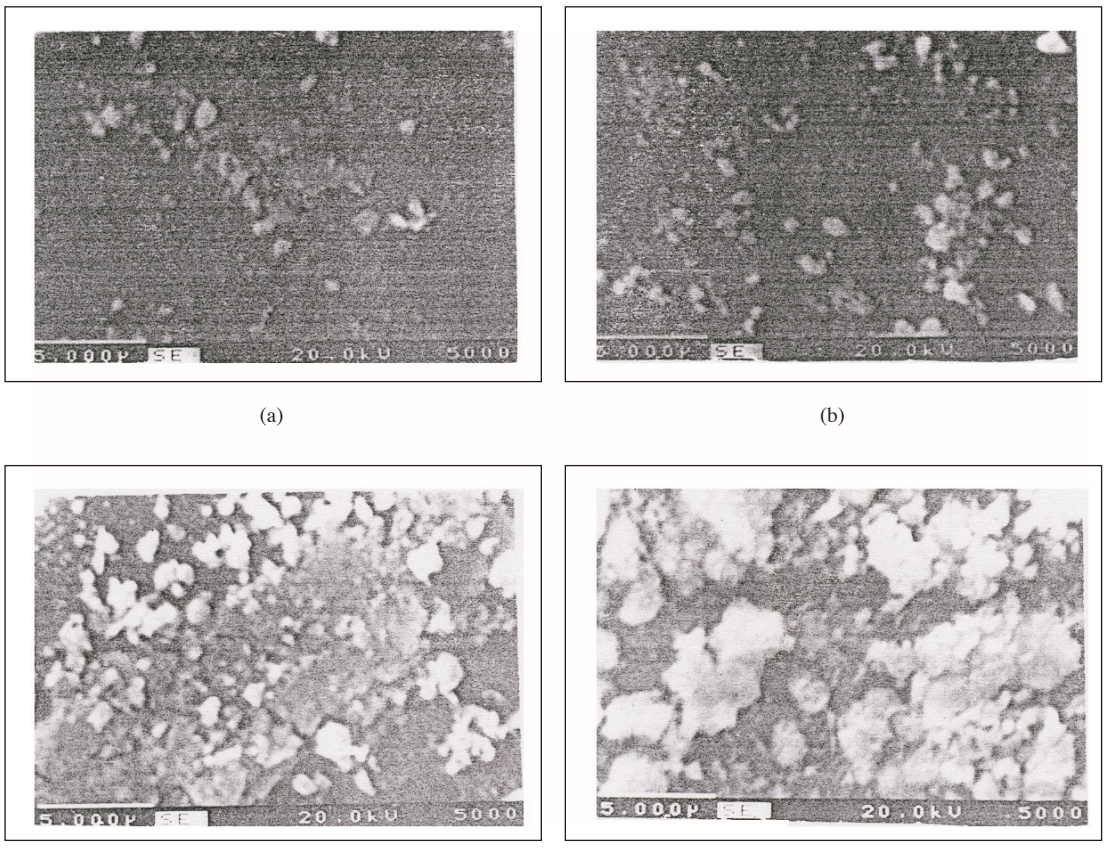

(a) (b)

(c) (d)

Figure 8. SEM micrographs of some of the typical $Hg_xCd_{1-x}Se$ photoelectrodes: x = 0, b) x = 0.005, c) x = 0.01, d) x = 0.02, e) x = 0.05 and f) x = 0.1.

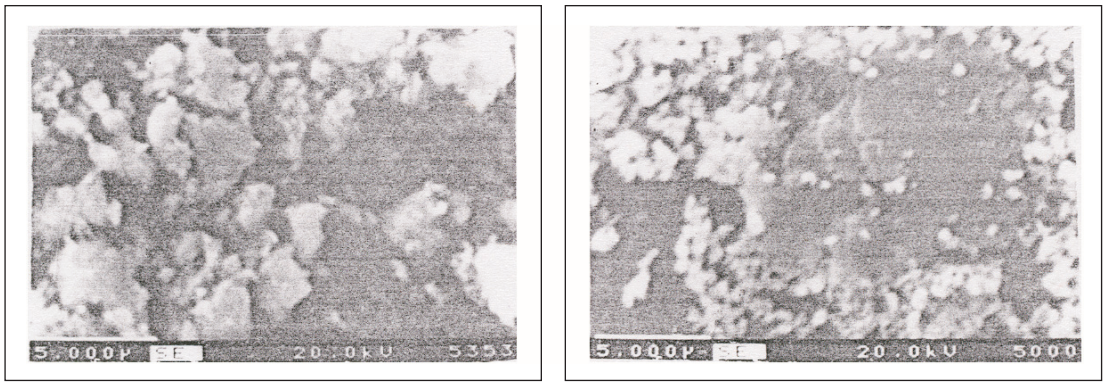

(e) (f)

Figure 8. Continued.

4. Conclusions

The chemical bath technique is found to be useful to synthesize $Hg_xCd_{1-x}Se$ thin film electrodes suitable for PEC applications. An attempt is made to investigate the various electrochemical properties as a function of the photoelectrode composition. The results indicated that the trace addition of mercury modified the photoelectrode properties, which consequently influences the various electrochemical properties of the cell. The cell performance is found to be improved and became optimum at x = 0.01. The enhancement in the open-circuit photopotential V_{ph} is ascribed to the increased flat-band potential V_{fb}, increased photoelectrode absorption and improved grain structures. The increase in short-circuit photocurrent I_{ph} is mainly due to the decrease in the photoelectrode resistance and band gap of the material and increased absorption of the incident light by the photoelectrode material.

Acknowledgements

I (VBP) am thankful to the authorities of Rayat Shikshan Sanstha, Satara, for allowing me for research as a teacher research fellow and Prin. A. S. Burungale, Karmaveer Bhaurao Patil College, Vashi, Navi Mumbai, for his constant inspiration, motivation and encouragement.

References

[1] K. Tsvekova and K. Kochev, *Sol. Ener. Mater.: Sol. Cells*, **31,** (1993), 429.

[2] G. S. Shahane, D. S. Sutrave and L. P. Deshmukh, *Ind. J. Pure Appl. Phys.,* **34,** (1996), 153.

[3] E. U. Masumdar, V. B. Pujari, V. S. Karande and L. P. Deshmukh, *J. of Mater. Sci.: Mater. in Elect.,* **14,** (2003), 43.

[4] L. P. Deshmukh and S. G. Holikatti, *J. of Phys. D Appl. Phys.,* **27,** (1994), 1786.

[5] L. P. Deshmukh and S. G. Holikatti, *ibid*, **33,** (1995), 763.

[6] S. H. Pawar and L. P. Deshmukh, *Ind. J. Pure Appl. Phys.,* **22,** (1984), 315.

[7] N. Hiemi and J. I. Muto, *J. of Mater. Sci.: Mater. in Elect.*, **11,** (2002), 145.

[8] L. P. Deshmukh, G. S. Shahane and K. M. Garadkar, *Ind. J. Pure Appl. Phys.,* **35**, (1997), 560.

[9] G. S. Shahane, B. M. More, C. B. Rotti and L. P. Deshmukh, *Mat. Chem. Phy.*, **47,** (1997), 266.

[10] V. B. Pujari, V. B. Gaikwad, E. U. Masumdar, P. D. More and L. P. Deshmukh, *Turk. J. of Phy.*, **26,** (2002), 407.

[11] V. B. Pujari, S. H. Mane, V. S. Karande, J. S. Dargad and L. P. Deshmukh, *Mat. Chem. Phy.,* **83,** (2004), 10.

[12] E. U. Masumdar, V. B. Pujari, V. B. Gaikwad, V. B. Patil and L. P. Deshmukh, *Eleventh International Workshop on the Physics of Semiconductor Devices, New Delhi, India,* Dec. 11-15, 2001

[13] A. Aruchamy, G. Aravamudan and G. V. Subbarao, *Bull. Mater. Sci.,* **4**, (1982), 483.

[14] K. Rajeshwar, P. Sing and J. Dubow, *J. of Electrochem. Soc.,* **128,** (1981), 1744.

[15] R. N. Noufi, P. A. Kohl, and A. J. Bard, *J. of Electrochem. Soc.,* **125,** (1978), 375.

[16] L. P. Deshmukh and G. S. Shahane, *Int. J. of Elect.,* **83**, (1997), 341.